Vol. 46 — N° 4 12 22 p. 735 – 749

GEOSTANDARDS and GEOANALYTICAL RESEARCH

Revisiting the Happy Jack Uraninite Reference Material: A Combined Electron Beam and Laser Ablation *In Situ* Study

Lingli **Zhou** (1, 2, 3)*, Thomas **Riegler** (3), Christophe **Bonnetti** (4), Sean **McClenaghan** (3) and Balz **Kamber** (3, 5)

(1) iCRAG, School of Earth Sciences, University College Dublin, Belfield, Dublin 4, Ireland
(2) Geological Survey Ireland, Beggars Bush, Dublin 4, Ireland
(3) iCRAG, School of Natural Sciences, Department of Geology, Trinity College Dublin, Dublin 2, Ireland
(4) State Key Laboratory of Nuclear Resources and Environment, East China University of Technology, Nanchang, Jiangxi, 330013, China
(5) School of Earth and Atmospheric Sciences Queensland University of Technology, Brisbane, QLD, 4001, Australia
* Corresponding author email id: lingli.zhou@icrag-centre.org

This new comprehensive *in situ* mineral-chemical characterisation of the Happy Jack uraninite has discovered additional information regarding matrix effects and trace element homogeneity, relevant to proposals that it could serve as a reference material (RM). On the LA-ICP-MS instrumentation used, there was an absence of discernible matrix effects relative to the silicate glass NIST SRM 610. Lanthanides and Y are found to be very homogeneously distributed in Happy Jack uraninite, Zr, Nb and Ti mass fractions reproducible but only within individual fragments, and other elements still generally heterogeneous. This means that the Happy Jack uraninite can serve as a secondary RM for quality control in studies of natural uraninites. In terms of absolute accuracy and intermediate measurement precision, the Happy Jack uraninite can be used for the homogeneous elements. For elements that are homogeneous within individual fragments only, intermediate measurement precision can still be evaluated, while information values will be obtained for the generally heterogeneous elements. Two distinct groups (high vs. low Zr) were distinguished to exist among different Happy Jack fragments in association with minor variation of REE mass fractions, which possibly explains the observed (heavy) REE discrepancy between *in situ* laser ablation and bulk solution ICP-MS analyses.

Keywords: reference material, uraninite, LA-ICP-MS, reference material development, REE.

Received 31 Jul 21 – Accepted 11 Aug 22

The emerging application of using uraninite chemistry as a provenance tool, both for ore genesis constraint (e.g., Pagel *et al.* 1987, Fryer and Taylor 1987, Keegan *et al.* 2008, Mercadier *et al.* 2011, Depiné *et al.* 2013, Lach *et al.* 2013, Frimmel *et al.* 2014, Alexandre *et al.* 2015) and forensic purposes (e.g., Spano *et al.* 2017), has increased the demand for high-precision characterisation of the chemical composition of uraninite. On the one hand, *in situ* techniques such as EPMA (electron probe microanalysis) and LA-ICP-MS (laser ablation-inductively coupled plasma-mass spectrometry) analyses are already being applied to examine the chemical signature of uraninite, exploiting advantages of precise determination of the mass fractions of a large range of elements on a basis of simple sample preparation process that eliminates contamination or mixing of geological records (Sylvester 2008a). On the other hand, development of a well-characterised uraninite reference material still needs refinement to achieve high-quality uraninite geochemical data by *in situ* techniques. The commonly used reference material to determine trace element mass fractions in uraninite samples is the silicate glass RM NIST SRM 610. Being of very different bulk composition to uraninite (uranium dioxide) a "matrix" or "matrix-matching" effect may affect instrument calibration depending on analytical settings (e.g., laser fluence) (Sylvester 2008b). Responding to the need for a suitable reference material, the well characterised Mistamisk uraninite was previously suggested for *in situ* analysis of uraninite samples (Kish and Cuney 1981, Bonhoure *et al.* 2007, Lach *et al.* 2013). A more recent careful study conducted by Dorais *et al.* (2020) re-examined the Mistamisk uraninite and compared it with the Happy Jack uraninite as a

doi: 10.1111/ggr.12457

reference material, applying several *in situ* and bulk analytical methods for the investigation of elemental abundance and heterogeneity. The work by Dorais *et al.* (2020) showed that both Ca and the rare earth elements (REE) contents are less variable in the Happy Jack uraninite than in the Mistamisk uraninite, and that the Happy Jack uraninite may be very suitable as a reference material for *in situ* analysis of U-rich materials, in particular, to characterise the REE signature of uranium ore concentrates and uraninite ores.

This study aimed to build on the work carried out by Dorais *et al.* (2020) in three ways. Firstly, to conduct an in-depth *in situ* investigation of mass fractions and homogeneity of forty trace element analytes in one Happy Jack uraninite fragment. Secondly, to investigate the effects, if any, of mineral inclusions within Happy Jack uraninite. This was motivated by the observation that bulk digested solution analysis trace element data by Dorais *et al.* (2020) slightly deviate from in situ data obtained in the same and our own study. We combined SEM-EDS and LA-ICP-MS spot and elemental mapping, with selective extraction of silicate inclusion data from 2D elemental map pixel arrays (Petrus *et al.* 2017). Thirdly, the extent of the "matrix-matching" effect was tested by comparison with NIST SRM 610 and analysis of a further massive uraninite.

It was found that the obtained REE mass fractions for Happy Jack are consistent at the scale of individual fragments, however, two distinct groups (high vs. low Zr, Nb and Ti) were distinguished to exist among different fragments, associated with minor variation of REE mass fractions. Elements like Fe and Cu are heterogeneous on an even smaller scale, which is likely due to inclusions of other phases, rather than being incorporated into the uraninite crystal structure. It is recommended that a primary characterisation of specific Happy Jack fragments is essential before using them as a reference material.

Experimental

Materials and experiment design

The Happy Jack uraninite fragment (approximately 5 mm × 5 mm × 4 mm, Appendix S1) for this study is originally from the Happy Jack mine in the White Canyon area, San Juan County, Utah, and was kindly provided by Dr Loretta Corcoran from the Department of Civil and Environmental Engineering and Earth Sciences at University of Notre Dame Indiana, USA. Foundation work, geochemical and geochronological work, leading to the development of the Happy Jack uraninite reference material by Dorais *et al.* (2020), can be found in articles by Corcoran *et al.* (2019) and Corcoran and Simonetti (2020). The Happy Jack uraninite fragment used for this study is from one of the three pieces reported in Dorais *et al.* (2020).

The uranium mineralisation of the Happy Jack mine is hosted by the Shinarump conglomerate of Upper Triassic Chinle Formation. The Shinarump conglomerate consists of beds of coarse- to fine-grained quartzose sandstone, conglomerate, siltstone and claystone. The ore body appears in both layered beds and replacement bodies. In general, the ore consists of an intergrowth of uraninite with copper sulfides, associated with minor secondary minerals of uranium and copper. Uraninite is the primary ore mineral of uranium in the Happy Jack deposit. It typically occurs in replacement of plant fragments and as cement of quartz grains (Miller 1955, Trites and Chew 1955). As a result, although massive in appearance, the uraninite is typically rich in very small inclusions of silicates and sulfides at the microscopic scale. For this study, a slice of the massive Happy Jack uraninite fragment (measuring approx. 5 mm x 5 mm in surface) was cut and mounted on a 1-inch resin block for microscopy observation and *in situ* geochemical analysis. The mounted sample was imaged under reflected light on an automated Nikon optical microscope at the Centre of Microscopy Analysis, Trinity College Dublin. Areas of interests were selected from the mounted sample for the subsequent SEM-EDS and LA-ICP-MS analyses.

Fifty spots distributed across the mounted Happy Jack uraninite slice were selected for the *in situ* LA-ICP-MS spot analysis, in order to determine the mass fractions of trace elements and investigate the chemical spatial variation (i.e., repeatability). The mass fractions of REE of the Happy Jack uraninite measured from this study were compared with the values reported by Dorais *et al.* (2020) to assess reproducibility and homogeneity. In addition, both SEM-EDS and LA-ICP-MS element mapping analyses were carried out on the Happy Jack uraninite to investigate the material's chemical homogeneity. The integration of the quantitative and qualitative analyses allows for an effective evaluation of the nature of Happy Jack uraninite as a reference material. An understanding of matrix matching effects was achieved by applying the Happy Jack uraninite as the "external" reference material for *in situ* measurement of the trace element mass fractions of NIST SRM 610 by LA-ICP-MS spot analysis. NIST SRM 610 was treated as an anonymous sample for which ten spots were analysed. The measured trace element mass fractions of NIST SRM 610 acquired from this study were then compared with the working values presented in Pearce *et al.* (1997). Finally, the Happy Jack uraninite RM, together with NIST SRM 610, were employed as the calibration ("external") reference materials for *in situ*

measurement of the trace element mass fractions of a further massive uraninite ore from the Rum Jungle uranium mine, Australia. The Rum Jungle uraninite sample was provided by the Geological Museum, Trinity College Dublin. This approach was employed to assess whether different uraninites show consistent matrix matching effects.

SEM-EDS

A first evaluation of the spatial homogeneity of the Happy Jack uraninite fragment was performed to inform planning of the LA-ICP-MS work. Analytical work was carried out at the Centre of Microscopy Analysis, Trinity College Dublin, using a Tescan field emission gun (FEG)-SEM equipped with two Oxford Instruments X-Max^N 150 mm^2 energy dispersive spectrometers (EDS) to produce chemical maps up to the scale of the entire resin-blocks covering areas up to several square centimetres at a micron-scale resolution. The EDS signal was processed with the Oxford Instruments Aztec software, and the analytical conditions were routinely set at 20 kV, with 1 nA beam current for spots and maps, respectively. Live counting time on spots were set at 15 milliseconds (ms) per pixel to obtain several tens of thousands of processed X-ray counts per pixel, thus favouring spectrum resolution over X-Ray count throughput achievable at lower processing time. The dead time was maintained between 30 and 40%. Semi-quantitative chemical maps were obtained by producing a montage of individual X-ray maps at a spatial resolution of 5 μm by 5 μm. This particular care in adjusting the processing time to resolve the potential interferences related to the analysis of a U-rich material is following a methodology developed for the large-scale EDS X-ray mapping on a mineralogically complex uraninite-bearing vein sample (Bonnetti *et al.* 2018). Spatial resolution was adjusted following the recommendations of Friel and Lyman (2006). Elements were routinely calibrated on natural reference materials in particular for spot analysis. For this study, natural pyrite, monazite, apatite, barite, augite, anorthoclase, microcline, olivine and rutile from the Smithsonian Microbeam Standard (Jarosewich 2002) and Astimex Standard Limited, Toronto, were used for the calibration of S, Fe, Si, Al, Mg, Mn, K, Na, Ca, Ba, Ti, P, Ce, La, Pr, Nd, Th mass fractions; pure metals (Ag, Au, Bi, Cu, Sb, Pb, Zn) and synthetic reference materials (InAs, PbTe) were also combined for the use of calibrations during the analysis (e.g., Riegler and McClenaghan 2017, Zhou *et al.* 2020).

Laser ablation (LA)-ICP-MS

On the basis of SEM-EDS analysis results, a total of fifty spots and one mapping area (size 1.0 × 0.8 mm) on the Happy Jack uraninite sample were analysed for element mass fractions and distribution by LA-ICP-MS. The LA-ICP-MS spot and element mapping analyses were carried out at the iCRAG LA-ICP-MS laboratory at Trinity College Dublin. The instrument consisted of a Photon machines G2 193 nm UV laser with a HelEx two-volume cell coupled to a Thermo iCAP Q ICP-MS. The ARIS (Aerosol Rapid Introduce System) capillary was applied to the elemental mapping in order to improve the mapping efficiency by enhancing material transport efficiency and reducing washout time (e.g., Zhou *et al.* 2017, 2020, Bonnetti *et al.* 2020). NIST SRM 610 and Happy Jack uraninite were selectively used as the "external" reference material during the *in situ* measurement of samples, depending on the design of experiment. The reported Ca content in the Happy Jack uraninite (1.93% *m/m*, Dorais *et al.* 2020) and the measured Ca content of the Rum Jungle uraninite by SEM-EDS (1.54% *m/m*) was used as the internal element index to calibrate the trace element mass fractions of the two uraninite samples, respectively. The Ca content of NIST SRM 610 (8.21% *m/m*) given by Pearce *et al.* (1997) was applied. The raw data were processed with the software Iolite v3.75 using the trace element data reduction scheme (Paton *et al.* 2011).

The laser fluence was set at 0.90 J cm^{-2} for both the spot and mapping analyses. A laser spot size of 20 μm^2 square and a repetition rate of 5 Hz was used for the spot analysis. The total acquisition time for each analysis was 60 s, comprising 40 s of sample ablation followed by 20 s background measurement. A sum of forty isotopes were monitored and measured for the mass fractions. The element list and dwell time of each analyte were ^{42}Ca (25 ms), ^{24}Mg (20 ms), ^{27}Al (20 ms), ^{29}Si (20 ms), ^{47}Ti (25 ms), ^{51}V (10 ms), ^{53}Cr (20 ms), ^{57}Fe (25 ms), ^{59}Co(20 ms), ^{60}Ni (20 ms), ^{66}Zn (20 ms), ^{75}As (25 ms), ^{89}Y (5 ms), ^{90}Zr (10 ms), ^{93}Nb (20 ms), ^{95}Mo (25 ms), ^{107}Ag (20 ms), ^{139}La (20 ms), ^{140}Ce (5 ms), ^{141}Pr (20 ms), ^{146}Nd (20 ms), ^{147}Sm (20 ms), ^{153}Eu (20 ms), ^{157}Gd (20 ms), ^{159}Tb (20 ms), ^{163}Dy (20 ms), ^{165}Ho (20 ms), ^{166}Er (20 ms), ^{169}Tm (20 ms), ^{172}Yb (20 ms), ^{175}Lu (20 ms), ^{181}Ta (20 ms), ^{182}W (20 ms), ^{197}Au (20 ms), ^{206}Pb (2 ms), ^{207}Pb (10 ms), ^{208}Pb (10 ms), ^{209}Bi (10 ms), ^{232}Th (20 ms) and ^{235}U (5 ms). For the element mapping analysis, a laser spot size of 20 μm^2, a scan speed of 20 μm s^{-1} and a repetition rate of 10 Hz were applied. The same element list was used for the mapping analysis, whereas the dwell time of analytes varied. During the mapping analysis, the dwell time was set at 15 ms for all the analytes except for ^{206}Pb, ^{207}Pb, ^{208}Pb and ^{235}U, which were assigned a dwell time of 20 ms each. The element maps of the Happy Jack uraninite presented in this study are fully quantified, employing NIST SRM 610 as the calibration reference material and the Ca content (1.93% *m/m*, Dorais

et al. 2020) as the internal element index. The descriptive parameters of the datasets were generated with the software SPSS.

Results and discussion

Material homogeneity

The Happy Jack uraninite shows a massive texture and a lack of internal zoning patterns judging from the BSE image, although abundant fractures and minor secondary mineral phases are visible from the reflected light microscopy image (Figure 1a). The SEM-EDS major element maps reveal that U is evenly distributed in the uraninite matrix (Figure 1b), and the secondary minerals are sulfide phases rich in Cu and Fe (Figures 1c, d). Some of the Cu-rich sulfide phases are oxidised and show distinct bluish colour under reflected light, suggesting covellite (Figure 1a). The observation of our study is identical to that reported by Dorais *et al.* (2020) who investigated three separated fragments of the Happy Jack uraninite. The homogeneous distribution of both U and Ca in the Happy Jack uraninite is essential to produce accurate compositional data when using either element as an internal element index for raw data processing. Moreover, the impurities in the Happy Jack uraninite are visible under optical microscope and can therefore be readily avoided during *in situ* measurement.

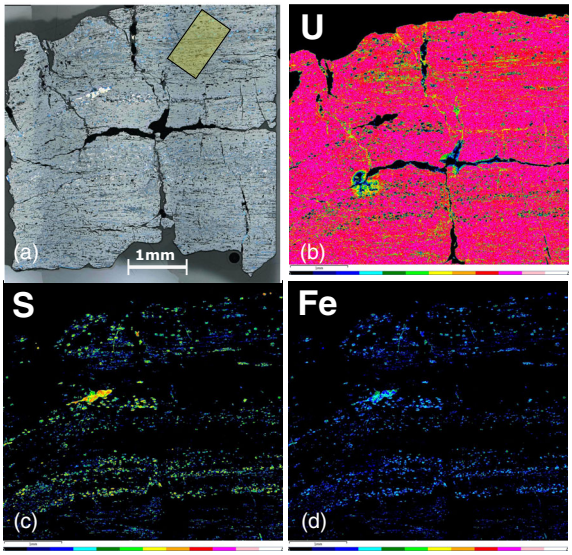

Figure 1. Happy Jack uraninite under (a) reflected light and by SEM-EDS element mapping showing the distribution of elements that are above the detection limits, including (b) U, (c) S and (d) Fe. The left hand end of the scale bars represents low mass fraction of the element; the mass fraction increases towards the right. The rectangle in (a) highlights the area analysed by LA-ICP-MS for elemental mapping.

Trace element distribution

Among the forty isotopes analysed, thirty-seven showed detectable signals, whereas the mass fractions of Ni, Ta and Au are generally below their LA-ICP-MS detection limits of 4.21 μg g^{-1}, 0.024 μg g^{-1}, 0.106 μg g^{-1}, respectively (Appendix S1 and Table 1). Silica had very high background signals during the measurement due to the use of N_2 to enhance ionisation efficiency, which resulted in a high detection limit of 2750 μg g^{-1}. The REE (La-Lu) show appreciable mass fractions for all the spot analyses, together with small standard deviation values. The value of ∑REE ranges from 7300 μg g^{-1} to 8850 μg g^{-1}, with an average of 8077 μg g^{-1}. Yttrium was constantly detected and is moderately enriched (1690 ± 92 μg g^{-1}). The chalcophile elements (Ag, Bi, and Zn) are detectable on occasions, most likely because these elements are mainly associated with the sulfide mineral inclusions. Arsenic is an exception, showing a relatively narrow range of mass fractions for the fifty spots (122–306 μg g^{-1}). In addition to the REE, the lithophile elements (Al, Mg, Cr, Fe, Zr, V, Nb) were all detectable, except that the Th mass fraction was close to the detection limit of 0.03 μg g^{-1}. The low ∑REE and extreme depletion of Th contents in the Happy Jack uraninite is indicative of a low-temperature hydrothermal origin, which agrees with the geological context of its genesis (Miller 1955, Trites and Chew 1955). The transition elements Co and Mo have mean mass fraction values of 3.1 and 64 μg g^{-1}, respectively, although the standard deviations are high (2.9 and 44 μg g^{-1}, respectively). Because the Pb-isotope composition of the uraninite is very different from the common Pb in NIST SRM 610, the Pb mass fraction cannot be quantified by measurement of an individual isotope. For example, taking the ^{206}Pb analyte yields an apparent Pb mass fraction of 18500 μg g^{-1} whereas ^{208}Pb yields an apparent mass fraction of only 280 μg g^{-1}. To cancel the isotope effect, the signals of all three determined Pb isotopes was summed to yield a Pb mass fraction of 2082.25 ± 1041.28 μg g^{-1}.

The REE mass fractions of the Happy Jack uraninite acquired from both this study and Dorais *et al.* (2020) are plotted in upper continental crust-normalisation (McLennan 2001) in Figure 2. The two separate datasets of measurement are highly comparable, showing similar enrichment relative to the upper continental crust values and uniform normalised distribution curves featuring a relatively smooth and flat REE distribution, minor fractionation of LREE over HREE, and very weak Eu anomalies (Figure 2a).

Table 1.
Element mass fractions of the Happy Jack uraninite fragment from this study, determined by LA-ICP-MS spot analysis

Analyte	*N*	Minimum	Maximum	Mean	2*s*
Mg (μg g^{-1})	50	21.50	62.50	38.23	10.53
Al (μg g^{-1})	50	139.30	5000.00	617.40	727.81
Si (μg g^{-1})	16	2400.00	4900.00	3136.88	638.40
Ti (μg g^{-1})	48	4.60	41.60	15.13	12.10
V (μg g^{-1})	50	3290.00	4190.00	3657.40	199.17
Cr (μg g^{-1})	50	10.30	19.00	14.08	1.74
Fe (μg g^{-1})	49	2191.00	20100.00	3126.20	2504.09
Co (μg g^{-1})	46	0.39	15.20	2.07	2.86
Ni (μg g^{-1})	10	3.60	18.10	7.06	4.35
Zn (μg g^{-1})	45	6.00	80.00	27.37	16.60
As (μg g^{-1})	50	121.60	306.00	230.03	43.49
Y (μg g^{-1})	50	1528.00	1886.00	1686.88	91.73
Zr (μg g^{-1})	50	1355.00	1736.00	1549.70	94.58
Nb (μg g^{-1})	50	8.83	10.87	9.76	0.43
Mo (μg g^{-1})	50	1.68	189.00	51.84	44.37
Ag (μg g^{-1})	26	0.15	217.00	28.38	51.97
La (μg g^{-1})	50	17.97	23.34	19.81	1.29
Ce (μg g^{-1})	50	1167.00	1525.00	1317.96	85.62
Pr (μg g^{-1})	50	273.00	340.00	308.88	15.71
Nd (μg g^{-1})	50	1380.00	1670.00	1560.20	63.55
Sm (μg g^{-1})	50	411.00	489.00	444.14	18.76
Eu (μg g^{-1})	50	135.10	163.90	146.04	6.03
Gd (μg g^{-1})	50	371.00	457.00	401.66	17.79
Tb (μg g^{-1})	50	80.70	95.80	86.76	3.50
Dy (μg g^{-1})	50	552.00	655.00	588.66	25.40
Ho (μg g^{-1})	50	107.50	131.80	117.23	5.17
Er (μg g^{-1})	50	297.00	365.00	321.58	16.80
Tm (μg g^{-1})	50	45.90	56.60	49.41	2.43
Yb (μg g^{-1})	50	328.00	405.00	352.30	16.61
Lu (μg g^{-1})	50	35.80	44.50	39.51	1.92
Ta (μg g^{-1})	14	0.00	0.04	0.02	0.01
W (μg g^{-1})	50	44.00	83.80	54.31	7.50
Au (μg g^{-1})	1	0.08	0.08	0.08	
^{206}Pb (μg g^{-1})	50	9810.00	40100.00	18518.60	5644.46
^{207}Pb (μg g^{-1})	50	671.00	2920.00	1287.88	458.17
^{208}Pb (μg g^{-1})	50	85.20	870.00	279.65	169.90
Bi (μg g^{-1})	10	0.06	0.41	0.17	0.11
Th (μg g^{-1})	19	0.02	0.23	0.10	0.07

N represents valid number of analyses for the statistical description; the total number of spot analyses was fifty. The complete dataset is provided in Appendix S1.

The material homogeneity is additionally reflected from the small variations of the REE mean values between the two datasets (Figure 2b). The majority of the REE mass fractions measured by Dorais *et al.* (2020) fall within or close to 10% variation relative to the data from this study (Figure 2c). The Happy Jack fragment analysed in this study shows a tighter distribution of REE mass fractions (i.e., smaller standard deviation) relative to the values reported by Dorais *et al.* (2020) (Figure 2d and Table 2). Quantitatively, the fifty measurements of the REE mass fractions in the Happy Jack uraninite performed in this study yielded smaller standard deviation values for each individual analyte, in particular for the LREE, in comparison with the previous *in situ* LA-ICP-MS measurement using a 213 nm wavelength laser (Figure 2b and Table 1). This may be attributed to the instrumentation and operation conditions such as the sensitivity of instruments and varied setting parameters (e.g., laser spot size, dwell time of analytes) during data acquisition. For instance, sample particles produced with 193 nm ablation are suggested to be smaller and more uniform than those with 213 nm ablation, leading to more complete ionisation in the plasma of ICP-MS (Sylvester 2008b). The low laser fluence employed in our study may also have reduced melting of samples and therefore prevented formation of large melt particles that experience incomplete vaporisation in the Ar plasma.

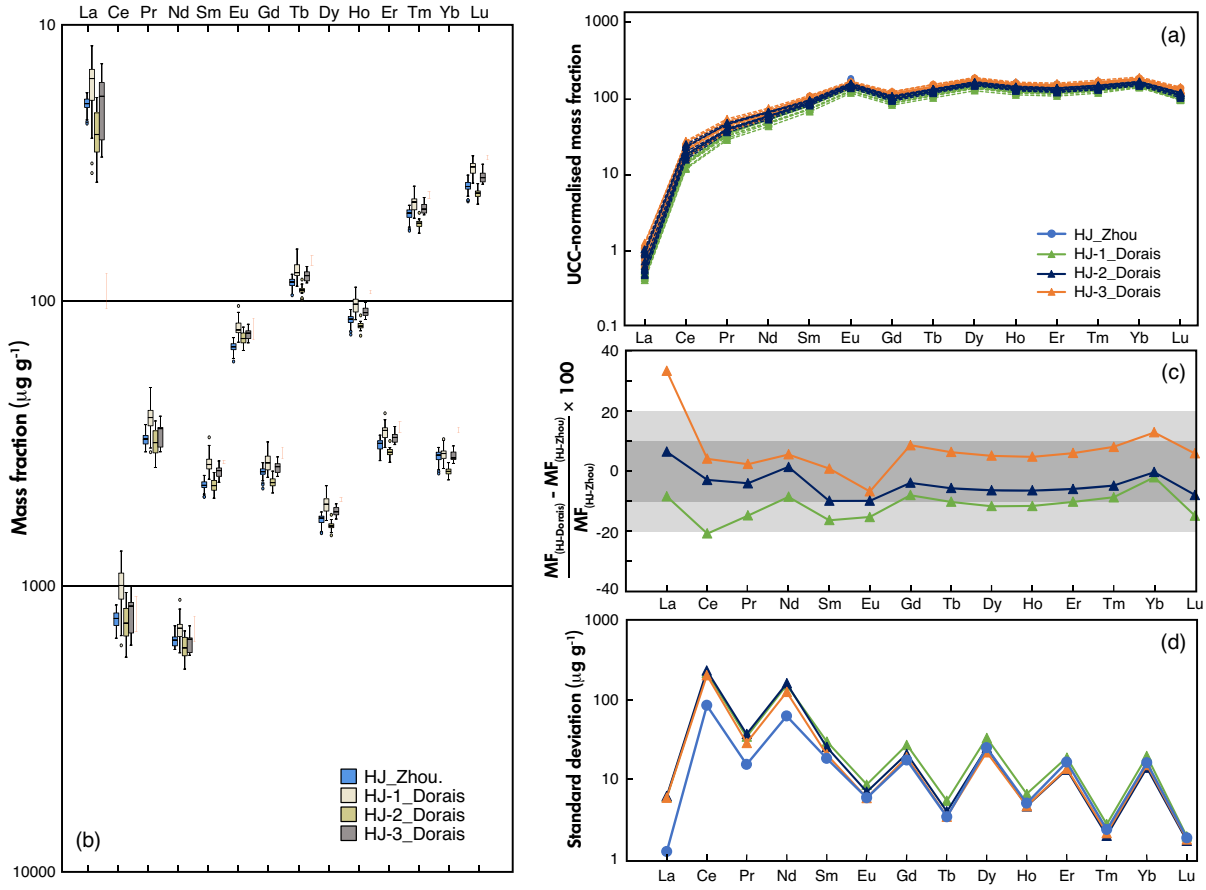

Figure 2. (a) Upper Continental Crust (UCC)-normalised REE patterns for the Happy Jack uraninite determined by LA-ICP-MS. HJ_Zhou represents the Happy Jack uraninite fragment measured for this study, and a total number of fifty spot analysis was carried out. HJ-1_Dorais, HJ-2_Dorais, and HJ-3_Dorais. represent the three Happy Jack uraninite fragments (section 1, section 2 and section 3) being analysed by Dorais *et al.* (2020), for which a total of forty-seven spot analysis were carried out. (b) Clustered boxplot of the REE mass fractions of Happy Jack uraninite fragments measured by LA-ICP-MS from this study and Dorais *et al.* (2020), including fifty spot measurements for HJ_Zhou, twenty-one spot measurements for HJ-1_Dorais, fifteen spot measurements for HJ-2_Dorais, and eleven spot measurements for HJ-3_Dorais. (c) Comparison of the REE mass fractions measured from *in situ* LA-ICP-MS spot analysis by this study and Dorais *et al.* (2020), which shows that the variations are mostly within 10% vicinity. (d) Comparison of the standard deviation values for the REE measurement of Happy Jack uraninite fragments by this study, which shows a generally more constrained spread of REE mass fractions measured by this study.

To summarise, quantitative assessment of REE mass fractions measured from separate pieces of Happy Jack uraninite on different instruments suggests that REE are homogeneous in the Happy Jack uraninite.

Trace element distribution

An area of 1.0 × 0.8 mm in size (Figure 1) was chosen for the LA-ICP-MS element mapping to further determine the material homogeneity of the Happy Jack uraninite. The fully quantified element maps of forty isotopes are presented in Figure 3. Consistent with the spot analysis results, the mapped area constantly shows depletion of Si, Ti, Ta, Au, and Bi. The distribution of Cr is not even, and its mass fraction in the Happy Jack uraninite is relatively low. The chalcophile elements (Ag, As and Zn) and the transition metal elements (Co, Ni and Mo) have similar distribution patterns, suggesting that these elements are associated with the included sulfide mineral phases. Lead (Pb) isotope mass fractions are detectable across the mapped area. Significant local enrichment of Pb corresponds to the occurrence of sulfide mineral phases. The same applies to Fe, which yields

Table 2.
Descriptive statistics of the measured REE mass fractions of the NIST SRM 610 determined by LA-ICP-MS spot analysis

This study						NIST SRM 610 reference values of Pearce *et al.* (1997) (μg g^{-1})
Analyte	*N*	Minimum	Maximum	Mean	2*s*	
La (μg g^{-1})	10	448	512	489.9	23.14	457 ± 144
Ce (μg g^{-1})	10	449	515	478.2	20.46	448 ± 34
Pr (μg g^{-1})	10	437	475	451.3	13.43	430 ± 60
Nd (μg g^{-1})	10	432	475	451.8	12.54	431 ± 76
Sm (μg g^{-1})	10	451	492	474.4	13.28	451 ± 42
Eu (μg g^{-1})	10	449	500	478.3	17.83	461 ± 104
Gd (μg g^{-1})	10	449	486	467.4	13.18	444 ± 42
Tb (μg g^{-1})	10	442	482	466.8	14.71	443 ± 44
Dy (μg g^{-1})	10	425	461	446.0	11.60	427 ± 36
Ho (μg g^{-1})	10	462	491	478.1	10.81	449 ± 50
Er (μg g^{-1})	10	440	473	454.4	11.39	426 ± 48
Tm (μg g^{-1})	10	418	454	437.6	13.33	420 ± 38
Yb (μg g^{-1})	10	439	485	467.4	13.80	445 ± 26
Lu (μg g^{-1})	10	434	486	460.9	16.99	435 ± 62

The dataset was produced by applying the Happy Jack uraninite as a reference material and a Ca content of 8.2144% *m/m* as an internal index for the trace element data reduction scheme in Iolite. The total number of spot analyses was ten. The complete dataset is provided in Appendix S1.

a consistent mass fraction of about 3000 μg g^{-1} across the mapped area while locally, the mass fraction reaches up to 6000 μg g^{-1}. The distribution of the lithophile elements Al and Mg is heterogeneous. Aluminium is generally depleted in the Happy Jack uraninite, and its local enrichment appears in stripes and associated with Mg enrichment, which we interpret as accumulations of minor silicate mineral inclusions. The distribution pattern of Mg is heterogeneous, complementing those elements associated with sulfide mineral phases. In contrast, the lithophile elements V, Nb and Zr demonstrate rather consistent distribution patterns at appreciable mass fractions. Tungsten (W) is evenly distributed excepting some local areas with elevated W. Ultimately, the REE demonstrate good homogeneity in the Happy Jack uraninite, which reflects their incorporation into the uraninite crystal structure (e.g., Mercadier *et al.* 2011).

The chemical maps show that, in addition to REE, Y, Zr and Nb are homogeneously distributed in the Happy Jack uraninite. Pertaining to this finding, we made a quantitative assessment of the homogeneity of Y, Zr and Nb in the Happy Jack uraninite by comparing our dataset with that of Dorais *et al.* (2020). The results show that Y is moderately enriched in the Happy Jack uraninite, and shows high repeatability and reproducibility for the data measured on different fragments and by different instruments, which is characterised by a comparable mean of Y (Figure 4a). Future investigation of the mass fraction of Y in the Happy Jack uraninite by bulk solution analysis will be a valuable addition for the assessment of its quality as a reference element. In contrast to Y, the mass fractions of Zr and Nb show a relatively large sample fragment-dependant variation and two end members were revealed (Figures 4a, b, c, Appendix S1). At the upper end of the obtained mass fractions are all the data measured for our Happy Jack fragment and those from section 2 sample of Dorais *et al.* (2020), whereas the more depleted values were measured for their section 1 and 3 samples. This inter-fragment heterogeneity does not limit the use of the Happy Jack uraninite as a secondary quality control RM but needs to be taken into account when comparing absolute values from different laboratories. The two distinct groups (high vs. low Zr) show a common linear correlation of Zr and Nb (Figure 4b), and similar linear correlation for Zr and Ti (Figure 4c). This is also reflected in a reasonably constant Zr/Nb ratio of 158.89 ± 8.44 analysed in our fragment (Appendix S1). In addition, an evaluation of Zr/Nb mass fraction ratios was made to see if the ratio is constant across all the Happy Jack fragments even when the absolute abundance is not. This comparison showed that there is much less variability in the Zr/Nb ratio across fragments than there is an absolute mass fraction of both Zr and Nb (Figure 4d). Elevated Zr mass fraction and positive

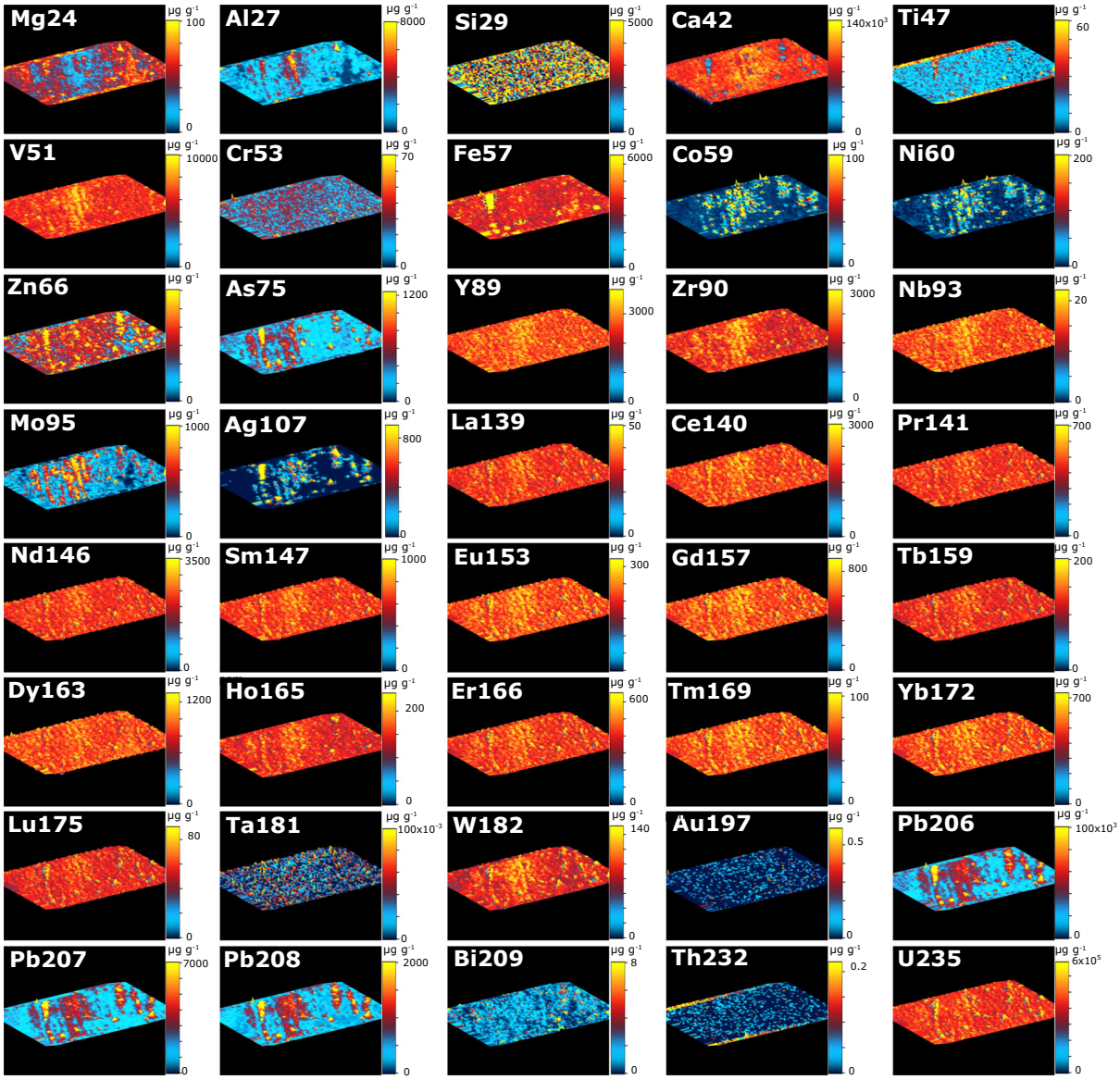

Figure 3. LA-ICP-MS element maps of the Happy Jack uraninite. The mapped area is about 1.0 × 0.8 cm^2 in size and indicated by the rectangle in Figure 1a.

correlation with Ti in uraninite could be caused by a pyroclastic volcanic contribution to the precursor sediments as U and Zr can be released during volcanic glass devitrification (e.g., Walton *et al.* 1981, Bonnetti *et al.* 2015, 2017). The occurrence of fine pyroclastic products formed during an episode of explosive volcanic activity was inferred for the Shinarump Formation, the host rock of Happy Jack uraninite (Waters and Granger 1963). The local enrichment of Zr, Nb and Ti in the Happy Jack uraninite is therefore interpreted to be source dependent, inherited from localised sediment chemistry variation (Mercadier *et al.* 2011, Lewis *et al.* 2020).

Happy Jack uraninite as a reference material

To evaluate the utility of the Happy Jack uraninite as a RM, it was tested as the calibrator for the measurement of trace element mass fractions in NIST SRM 610 by LA-ICP-MS spot analysis. The preferred values of the element (REE) mass fractions in the Happy Jack uraninite was derived from the previous fifty spot analyses of this study and represented by the mean values listed in Table 1. The trace element mass fractions of NIST SRM 610 measured in this way consistently fall within the range of certificated values (*CV*) as shown in Table 2 and illustrated in the boxplot of Figure 5. The

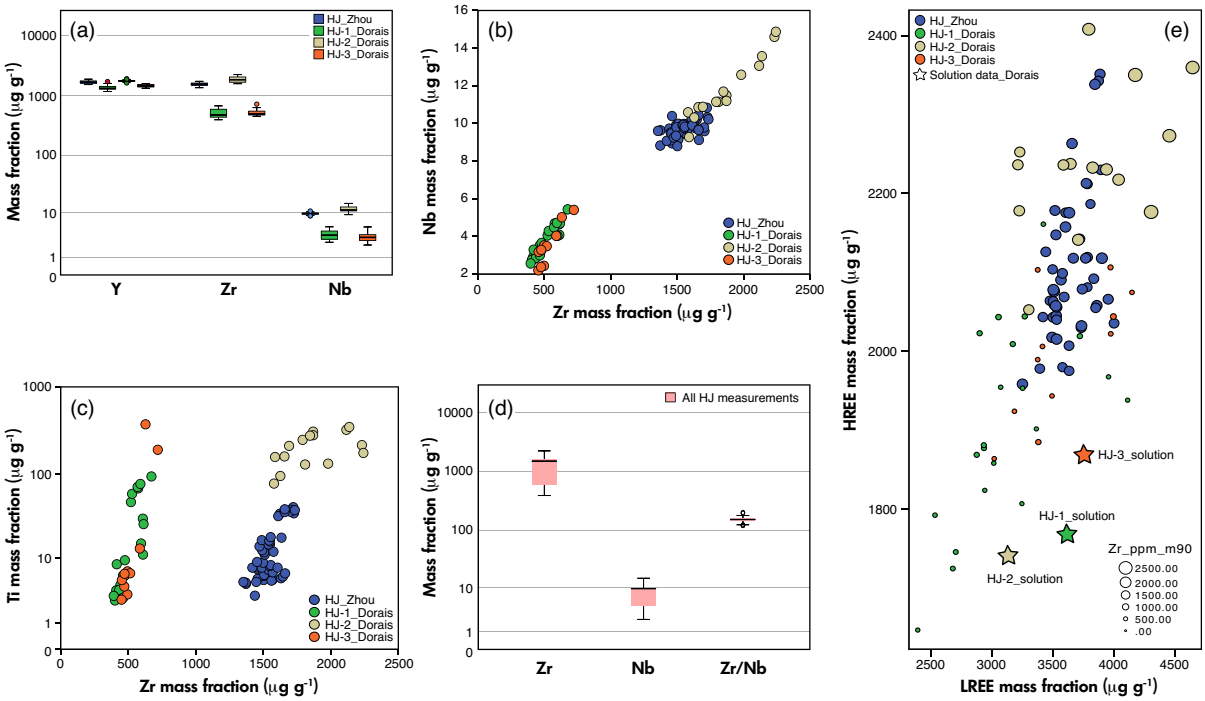

Figure 4. Comparison of the Zr, Nb and Ti mass fractions for all the Happy Jack uraninite fragments measured by *in situ* LA-ICP-MS spot analysis, which demonstrates a rather consistent Y mass fraction and Zr/Nb ratio, as well as outlines two distinct groups of Zr, Nb and Ti mass fractions in association with minor variations of REE mass fractions. (a) Boxplot of the measured Y, Zr and Nb mass fractions of the Happy Jack fragment from this study (HJ_Zhou) and from Dorais *et al.* (2020) (HJ-1_Dorais, HJ-2_Dorais, and HJ-3_Dorais). (b) Bivariate plots of mass fractions of Nb and Zr, which shows a common linear correlation. The two distinct groups are clearly outlined. (c) Bivariate plots of mass fractions of Zr and Ti, which shows a similar linear correlation. The linear correlation may suggest a contribution of pyroclastic volcanic in source materials as a reference material. (d) Boxplot of the measured Zr and Nb mass fractions and the Zr/Nb ratio of all the Happy Jack fragments, which displays a constant Zr/Nb ratio characterised with small standard deviation, as well as relatively a large variation of Zr and Nb mass fractions. (e) Bubble plots of the mass fractions of Zr, LREE and HREE, showing that the two distinct groups (high vs. low Zr) have minor differences of LREE and HREE mass fractions.

difference between the mean REE mass fractions from our measurements and the certified values are within uncertainty (Table 2).

Twenty-six measurements were further conducted on the Rum Jungle uraninite by *in situ* LA-ICP-MS spot analysis, exploiting both the Happy Jack uraninite and NIST SRM 610 as calibrators. The raw data of the Rum Jungle uraninite spot analysis was alternatively processed by applying the Happy Jack uraninite and NIST SRM 610 RMs, respectively, as the calibration reference material in the Iolite software. The twenty-six measurements of the Rum Jungle uraninite yielded highly comparable trace element mass fractions regardless of which calibrator was applied (Table 3 and Figure 6), and the two datasets are identical in the standard deviation value of individual analytes (Table 3). In summary, both the quality control (QC) check on NIST SRM 610 and the consistence of the two datasets for the Rum Jungle uraninite suggest that the Happy Jack uraninite shows desirable qualities as a reference material for *in situ* measurement of REE mass fractions in natural U-rich materials.

Lack of "matrix-matching" effect

Interestingly, despite the distinct chemical composition and physical nature of the NIST SRM 610 glass and uraninite, comparison of the aforementioned two datasets (Figure 6) shows very minor "matrix-matching" effect. This could have several reasons. Firstly, the internal

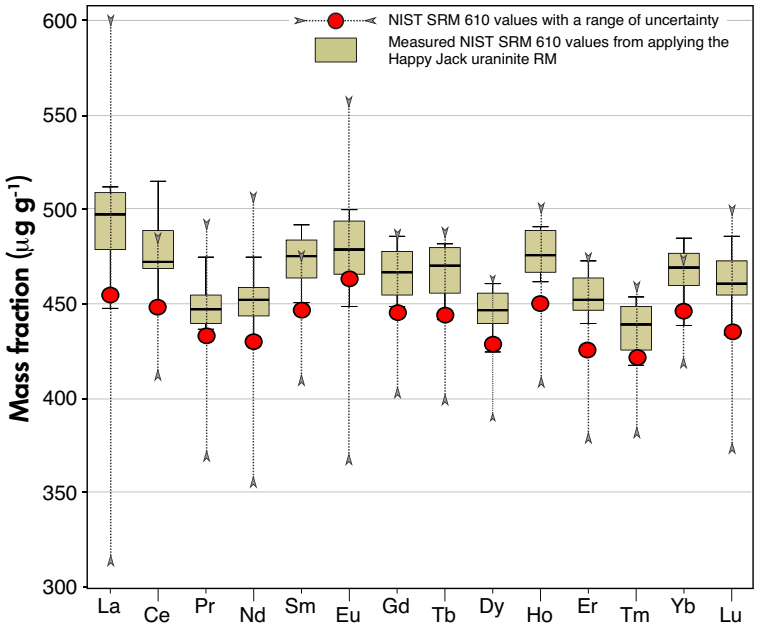

Figure 5. Boxplot of the measured REE mass fractions of NIST SRM 610 by employing the Happy Jack uraninite as a reference material. The values of REE mass fractions of NIST SRM 610 are represented by the red dots together with ranges of uncertainty (data source: Pearce *et al.* 1997). The complete dataset of our measurement results is included in Appendix S1.

Table 3.
Descriptive statistics of the REE mass fractions of the Rum Jungle uraninite determined by LA-ICP-MS spot analysis

Analyte	*N*	Applying the Happy Jack uraninite RM				Applying NIST SRM 610			
		Minimum	Maximum	Mean	2*s*	Minimum	Maximum	Mean	2*s*
La (μg g^{-1})	26	6.3	9.1	7.54	0.85	6.0	9.3	7.74	0.87
Ce (μg g^{-1})	26	33.0	54.1	40.62	5.55	32.0	52.9	39.73	5.43
Pr (μg g^{-1})	26	6.0	10.0	7.47	0.97	6.2	9.9	7.40	0.97
Nd (μg g^{-1})	26	42.0	62.4	49.50	5.85	40.0	60.6	48.04	5.69
Sm (μg g^{-1})	26	63.2	88.7	72.31	7.24	63.0	88.4	72.12	7.21
Eu (μg g^{-1})	26	14.0	18.1	15.61	1.32	14.0	18.4	15.89	1.34
Gd (μg g^{-1})	26	195.0	249.0	221.07	15.58	192.7	247.0	218.96	15.46
Tb (μg g^{-1})	26	55.0	69.5	61.74	4.23	55.0	69.2	61.47	4.21
Dy (μg g^{-1})	26	367.0	454.0	408.65	24.18	368.0	455.0	409.81	24.25
Ho (μg g^{-1})	26	58.0	69.3	63.74	3.52	56.6	67.5	62.11	3.44
Er (μg g^{-1})	26	116.0	140.7	128.74	7.34	113.5	138.0	126.30	7.20
Tm (μg g^{-1})	26	12.9	16.3	14.86	0.90	12.9	16.3	14.81	0.89
Yb (μg g^{-1})	26	75.5	96.8	86.02	5.32	74.5	95.5	84.87	5.25

Two datasets were produced by applying the Happy Jack uraninite RM and NIST SRM 610 as calibration reference materials, respectively. The measured Ca content of the Rum Jungle uraninite (1.54% *m/m*) was applied as an internal index. The total number of spot analyses is twenty-six. The complete dataset is provided in Appendix S1.

standardisation element Ca varies on the same order of magnitude in content for NIST SRM 610 (Ca = 8.2% *m/m*) and uraninite ores (up to 2.0% *m/m*). The small variation of the two values tends to reduce the K_{is} value, which is a parameter measuring the fractionation of internal standard elements caused by sensitivity drift, matrix effect and the difference in ablation yield between samples and reference materials (equation 3 in Lin *et al.* (2016) and Eggins

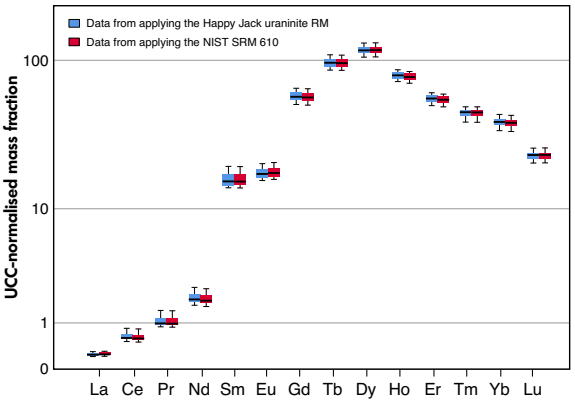

Figure 6. Clustered boxplot of the REE mass fractions of the Rum Jungle uraninite determined by LA-ICP-MS spot analysis. Two datasets are plotted for comparison, obtained by using the Happy Jack uraninite and NIST SRM 610 as the calibrating reference material.

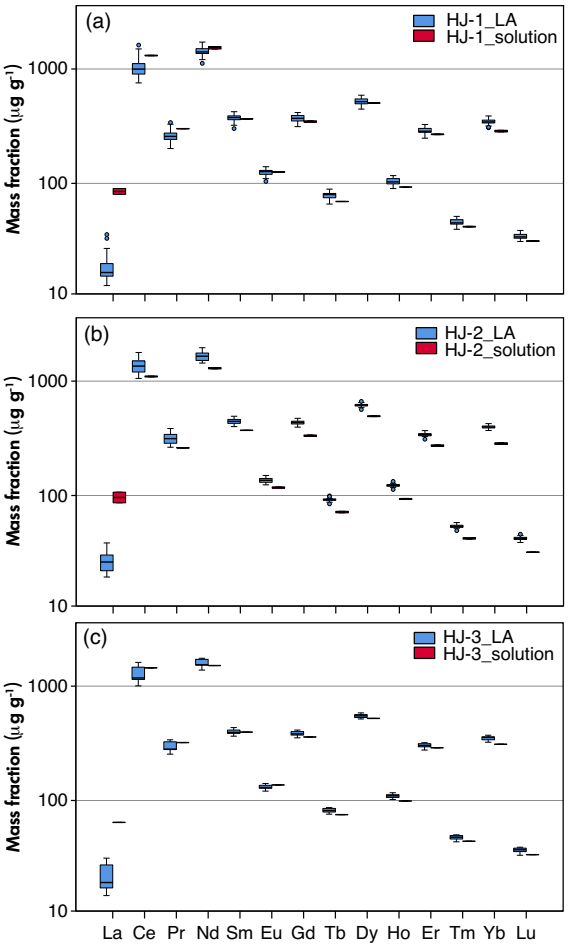

Figure 7. Clustered boxplots of the REE mass fractions of the three Happy Jack uraninite fragments measured by *in situ* LA-ICP-MS and bulk solution analyses (data source: Dorais *et al.* 2020). The comparison shows that there is a minor discrepancy of REE mass fractions by applying the two different measurement techniques. The number of measurements for the HJ-1_solution, HJ-2_solution and HJ-3_solution is two, two and one, respectively.

et al. (1997)), therefore achieving better corrections for variable "ablation yield" during laser sampling. The similar ionic radius of REE (approximately 1.06 Å) to Ca (1.06 Å) may also contribute to reducing the difference of fractionation behaviour of the internal standard element (i.e., Ca) and the determined elements (i.e., REE), and therefore minimising the "matrix-matching" effect. More importantly, the relative sensitivity of REE and Ca recorded by the mass spectrometer is observed to be similar for a group of elements in silicate minerals and glasses (Sylvester 2008b, Sindern 2017). The common substitution of Ca and REE in the structure of uraninite (Janeczek and Ewing 1992) can be explained by the similar ionic radius of REE (approximately 1.0 Å) and Ca (1.06 Å) to that of U (1.06 Å). The metal (REE, Y)-oxygen chemical bonds in the structure of uraninite may lead to comparable laser ablation behaviour to those in the tetrahedral and octahedral units in the structure of silicate minerals. Collectively, these factors may explain the very limited "matrix-matching" effect observed.

Although one original goal of the study was to test whether trace elements in uraninite needed a matrix-matched RM and if so, to evaluate a greater number of elements in the Happy Jack as potential reference concentrations, it turned out that accurate mass fraction data for uraninite can be obtained using NIST SRM 610 as the calibration RM. This is at least true with the instrumental setup, ablation parameters and tuning setting employed in this study. Analysts should, however, not *a priori* assume this to be the case for every LA-ICP-MS setup. Thus, the Happy Jack can initially be used to test whether a particular LA-ICP-MS setup yields accurate data when analysed with NIST SRM 610 as the calibration RM. For instruments where this is not the case, the Happy Jack can serve as a calibration RM. For laboratories where no significant matrix effect is found, the Happy Jack uraninite makes a very good secondary RM for QC, to establish (long-term) intermediate measurement precision, and within session repeatability and accuracy. Such a robust analytical protocol is essential to accurately measure impurity concentrations in uranium materials for safe use of nuclear energy (Gadd *et al.* 2001, Peńkin 2016), to trace material origin (Frimmel *et al.* 2014, Alexandre *et al.* 2015) and to develop possible substitution of materials (Berthet and Ephritikhine 1998).

Table 4.
REE discrepancy between *in situ* laser ablation and bulk solution ICP-MS analyses identified in Dorais *et al.* (2020) and our suggested models to explain the discrepancy

Analyte	Bulk solution composition (Dorais *et al.* 2020)	Digestion of silicate mineral inclusion model			Internal metal zoning model		
	Mean (section 2 sample)	LA-ICP-MS spot analysis (this study) Mean (Happy Jack uraninite)	Monocle extraction (this study) Mean (Silicate mineral inclusions)	Required proportion (R) of Happy Jack uraninite relative to the silicate mineral inclusions in order to generate the bulk solution composition from digestion of the silicate mineral inclusions in the Happy Jack uraninite	Mean ($Zr > 1000$ $\mu g\ g^{-1}$ group)	Mean ($Zr < 1000$ $\mu g\ g^{-1}$ group)	Required proportion (R′) of the high Zr group Happy Jack uraninite relative to the low Zr group in order to generate the bulk solution composition from internal metal zoning
La	18.73	19.80	916.45	1.00119	21.3249	19.1453	-0.19054
Ce	1055.82	1317.96	56615.45	1.00474	1330.3354	1124.6109	-0.33438
Pr	264.93	308.88	12125.79	1.00372	310.5126	274.5631	-0.26796
Nd	1437.88	1560.20	64990.06	1.00193	1579.998	1479.5134	-0.41433
Sm	401.44	444.14	18717.78	1.00234	444.97	381.3891	0.31536
Eu	124.02	146.04	6148.13	1.00367	143.7478	126.3956	-0.13690
Gd	397.03	401.66	16660.69	1.00028	409.5722	374.98	0.63743
Tb	84.29	86.76	3571.42	1.00071	88.0174	79.2091	0.57683
Dy	564.81	588.66	24352.54	1.00100	595.5422	530.53	0.52729
Ho	112.76	117.23	4730.11	1.00097	118.5178	105.6728	0.55175
Er	311.46	321.58	12711.77	1.00082	325.9952	293.3506	0.55474
Tm	48.86	49.41	2017.64	1.00028	50.3189	45.7406	0.68134
Yb	370.95	352.30	13781.20	0.99861	362.7175	347.0222	1.52452
Lu	38.43	39.51	1549.34	1.00072	40.0355	34.5737	0.70605

REE discrepancy between *in situ* laser ablation and bulk solution ICP-MS measurements

Dorais *et al.* (2020) conducted both *in situ* laser ablation and bulk solution ICP-MS analyses of the Happy Jack uraninite and observed what they termed a minor discrepancy of REE content between the two approaches (Figures 7a, b, c). Reprocessing the REE data of Dorais *et al.* (2020) reveals, however, a significant enrichment of La ($Mean_{bulk\ solution/laser\ ablation}$ = 2.3–4.7) for the bulk solution ICP-MS analysis result, whereas the $Mean_{bulk\ solution/laser\ ablation}$ varies at around 1 for the heavier REE (Table 4). The HREE generally show depletions ($Mean_{bulk\ solution/laser\ ablation}$ = 0.8–1.02) in the bulk solution analysis. The likely reason for the REE discrepancy was attributed to the inclusion and digestion of minor mineral phases, i.e., sulfides and silicates (Dorais *et al.* 2020). To validate this hypothesis, we used the software tool Monocle (Petrus *et al.* 2017) to localise (Figure 1) and extract pixel data that are likely dominated by silicate mineral inclusions within the uraninite. To ensure accurate comparison, the extracted data were then only compared with the solution REE measurements for section 2 sample in Dorais *et al.* (2020), which based on identical Zr mass fractions (Figure 4e), was the likely parent of our fragment.

To extract element mass fraction pixels from the map dominated by silicate mineral phases a selection criterion of "Al_ppm_SQ_m27 > 20000 ppm" was set in Monocle. Due to the unknown Ca mass fraction of the sub-microscopic silicate inclusions, a generic sheet silicate Al mass fraction of 20% *m/m* was used for internal calibration of the REE mass fractions of the inferred silicate mineral phases (Appendix S1). Comparison of the REE mass fractions of the silicate mineral phases with the mean of Happy Jack uraninite provides an approximate quantitative assessment of the identified REE discrepancy. The result shows that the REE discrepancy between *in situ* laser ablation and bulk solution ICP-MS analyses cannot be readily explained by a mixing model solely involving silicate mineral inclusions since the required portion of Happy Jack uraninite relative to the silicate mineral inclusions in order to generate the bulk composition from digestion of silicate mineral inclusions is larger than 100% for all the REE except Yb (Table 4).

Alternatively, a minor internal REE variation, which was observed to be associated with the local enrichment of Zr (Figure 4e), can explain the observed HREE discrepancy between *in situ* and bulk solution analyses. A criterion of Zr content below or above 1000 μg g^{-1} was applied to the entire dataset to separate the two distinct groups (high vs. low Zr, Appendix S1). Means of the individual REE were calculated for the two groups of Happy Jack fragments, respectively, which were used for developing a mixing model. Calculation shows that supposing a Happy Jack uraninite sample is composed of approximately 70% high Zr and approximately 30% low Zr groups the mixing can account for the majority of HREE (except Eu) mass fractions measured by bulk solution analysis (Table 4). The deviation of LREE (La–Nd) from the mixing model may be caused by either unidentified mineral inclusion phases in the Happy Jack uraninite (e.g., sulfate) or measurement artefacts. For example, the lower atomic number REE (La–Nd) show a high variability during a study of matrix effect on the determination of REE in UO_2 by LA-ICP-MS, possibly caused by space-charge effect (Lach *et al.* 2013). To summarise, the REE discrepancy between *in situ* laser ablation and bulk solution ICP-MS analyses for the Happy Jack uraninite is likely caused by the internal heterogeneity of Happy Jack uraninite. It is essential that laboratories that receive a piece of the Happy Jack sample characterise their own fragments because the uncertainties for the REE concentrations published by previous studies likely represent an upper limit and the uncertainties within a single fragment are likely to be significantly more constrained.

Conclusions

This study presents a comprehensive characterisation of the mineralogy and geochemistry of the Happy Jack uraninite by *in situ* SEM-EDS and LA-ICP-MS analyses. On this basis we presented both qualitative and quantitative evaluations of the Happy Jack uraninite as a RM for the utilisation of laser-based technique in analytical spectrometry. In summary, we have observed homogeneity/heterogeneity in the Happy Jack uraninite on different scales. The REE are homogeneous over several fragments; Zr, Nb and Ti are homogeneous within a given small fragment; elements like Fe and Cu are heterogeneous on an even smaller scale, which is likely caused by inclusions of other phases rather than incorporation into the uraninite crystal structure.

More specifically, the main findings of this study are as follows. The Happy Jack uraninite fragment studied herein primarily comprises uraninite and minor Cu-Fe sulfide. Silicate mineral inclusions are visible under optical microscopy and can be readily avoided during *in situ* analysis but apparently do not affect bulk REE mass fractions. In addition to the major constitutional elements U and Ca, the Happy Jack uraninite fragment is characterised by homogenous distribution and moderate enrichment of a range of trace elements including the REE, Y, V, Nb and Zr. In comparison, the enrichment of Fe, Ag, As, Zn, Co, Ni, Mo and Pb is associated with the sulfide mineral inclusions in the Happy Jack uraninite. Magnesium, Al and Cr may be hosted in silicate mineral phases. Silica, Ti, Ta, Au, Bi and Th are generally depleted. The REE and Y mass fractions are rather consistent (mostly vary within 10%) across the different Happy Jack uraninite fragments, affirming that the Happy Jack uraninite is an appropriate QC RM for *in situ* LA-ICP-MS analysis of the mass fractions of REE in natural U-rich materials (e.g., uraninite ores). Zirconium outlines two distinct groups (high vs. low Zr) for the different Happy Jack fragments, associated with a major variation of Nb and Ti mass fractions and a minor variation of REE mass fractions. However, the homogeneity of Zr, Nb and Ti displayed at the scale of a given small fragment indicates the validity of applying the Happy Jack uraninite as a secondary QC RM for these elements by comparing standard deviations from repeated analysis on a given small fragment or assessing the (long-term) intermediate measurement precision in a laboratory by repeated analysis over several sessions. NIST SRM 610 shows trivial "matrix-matching" effect for the use of measuring REE mass fractions of different uraninite ores by LA-ICP-MS. A robust analytical protocol therefore relies on NIST SRM 610 as the primary RM and Happy Jack uraninite as the secondary QC RM for the analysis of REE mass fractions of uraninite ores and uranium ore concentrate samples. An internal heterogeneity (high vs. low Zr groups) of the Happy Jack uraninite can cause minor HREE discrepancy between laser ablation and bulk solution ICP-MS; LREE discrepancy is more likely to be induced by digestion of mineral inclusions and/or artefacts of measurement techniques. A primary mineralogical and geochemical characterisation at a fragment scale will be essential should a laboratory consider applying it as a reference material.

Acknowledgements

This research was funded by Science Foundation Ireland (SFI) Grant Number 21/PATH-S/9601, National Key Research and Development Program of China (2021YFC2900300) and Geological Survey Ireland (grant no. 2019-PD-90622_Zhou). We would like to thank Patrick Wyse Jackson, the curator of Geological Museum, Trinity College Dublin, for kindly providing the Rum Jungle uraninite sample for this study. The authors are also grateful for the constructive comments from reviewer 1 and the manuscript handling editor (Thomas Zack), which helped to improve the quality of this manuscript

substantially. Zhou LL would like to thank Foteini Drakou for help with part of the data processing and the journal managing editor Edward Williams for his time dealing with the manuscript. Corinne Dorais and Loretta Corcoran are also thanked for kindly donating the Happy Jack fragment to our study and subsequent communications on the origin of used materials. Open access funding provided by IReL.

Data availability statement

The data that support the findings of this study are openly available in the main text and online supporting information.

References

Alexandre P., Kyser K., Layton-Matthews D., Joy B. and Uvarova Y. (2015)
Chemical compositions of natural uraninite. Canadian Mineralogist, 53, 595–622.

Berthet J.C. and Ephritikhine M. (1998)
New advances in the chemistry of uranium amide compounds. Coordination Chemistry Reviews, 178, 83–116.

Bonhoure J., Kister P., Cuney M. and Deloule E. (2007)
Methodology for rare earth element determinations of uranium oxides by ion microprobe. Geostandards and Geoanalytical Research, 31, 209–225.

Bonnetti C., Cuney M., Malartre F., Michels R., Liu X. and Peng Y. (2015)
The Nuheting deposit, Erlian Basin, NE China: Synsedimentary to diagenetic uranium mineralization. Ore Geology Reviews, 69, 118–139.

Bonnetti C., Cuney M., Bourlange S., Deloule E., Poujol M., Liu X., Peng Y. and Yang J. (2017)
Primary uranium sources for sedimentary-hosted uranium deposits in NE China: Insight from basement igneous rocks of the Erlian Basin. Mineralium Deposita, 52, 297–315.

Bonnetti C., Liu X., Mercadier J., Cuney M., Deloule E., Villeneuve J. and Liu W. (2018)
The genesis of granite-related hydrothermal uranium deposits in the Xiazhuang and Zhuguang ore fields, North Guangdong Province, SE China: Insights from mineralogical, trace elements and U-Pb isotopes signatures of the U mineralisation. Ore Geology Reviews, 92, 588–612.

Bonnetti C., Zhou L., Riegler T., Brugger J. and Fairclough M. (2020)
Large S isotope and trace element fractionations in pyrite of uranium roll front systems result from internally-driven biogeochemical cycle. Geochimica et Cosmochimica Acta, 282, 113–132.

Corcoran L., Simonetti A., Spano T.L., Lewis S.R., Dorais C., Simonetti S. and Burns P.C. (2019)
Multivariate analysis based on geochemical, isotopic, and mineralogical compositions of uranium-rich samples. Minerals, 9, 537.

Corcoran L. and Simonetti A. (2020)
Geochronology of uraninite revisited. Minerals, 10, 205.

Depiné M., Frimmel H.E., Emsbo P., Koenig A.E. and Kern M. (2013)
Trace element distribution in uraninite from Mesoarchaean Witwatersrand conglomerates (South Africa) supports placer model and magmatogenic source. Mineralium Deposita, 48, 423–435.

Dorais C., Simonetti A., Corcoran L., Spano T.L. and Burns P.C. (2020)
Happy Jack Uraninite: A new reference material for high spatial resolution analysis of U-rich matrices. Geostandards and Geoanalytical Research, 44, 125–132.

Eggins S.M., Woodhead J.D., Kinsley L.P.J., Mortimer G.E., Sylvester P., McCulloch M.T., Hergt J.M., Handler M.R. (1997)
A simple method for the precise determination of ≥ 40 trace elements in geological samples by ICP-MS using enriched isotope internal standardisation. Chemical Geology, 134, 311–326.

Friel J.J. and Lyman C.E. (2006)
X-ray mapping in electron-beam instruments. Microscopy and Microanalysis, 12, 2–25.

Frimmel H.E., Schedel S. and Brätz H. (2014)
Uraninite chemistry as forensic tool for provenance analysis. Applied Geochemistry, 48, 104–121.

Fryer B.J. and Taylor R.P. (1987)
Rare-earth element distributions in uraninites: Implications for ore genesis. Chemical Geology, 63, 101–108.

Gadd P.S., Marshall K.M. and Blagojevic N. (2019)
Combining analytical techniques for trace elements in uranium oxide (U_3O_8). http://www.iaea.org/inis/collection/NCLCollectionStore/_Public/33/034/33034317.pdf

Jarosewich E. (2002)
Smithsonian microbeam standards. Journal of Research of the National Institute of Standards and Technology, 107, 681.

Janeczek J. and Ewing R.C. (1992)
Structural formula of uraninite. Journal of Nuclear Materials, 190, 128–132.

Keegan E., Richter S., Kelly I., Wong H., Gadd P., Kuehn H. and Alonso-Munoz A. (2008)
The provenance of Australian uranium ore concentrates by elemental and isotopic analysis. Applied Geochemistry, 23, 765–777.

Kish L. and Cuney M. (1981)
Uraninite-albite veins from the Mistamisk Valley of the Labrador Trough, Quebec. Mineralogical Magazine, 44, 471–483.

Lach P., Mercadier J., Dubessy J., Boiron M.C. and Cuney M. (2013)
In situ quantitative measurement of rare earth elements in uranium oxides by laser ablation-inductively coupled plasma-mass spectrometry. Geostandards and Geoanalytical Research, 37, 277–296.

references

Lewis S.R., Simonetti A., Corcoran L., Simonetti S.S., Dorais C. and Burns P.C. (2020)
The role of continental crust in the formation of uraninite-based ore deposits. **Minerals**, **10**, 136.

Lin J., Liu Y., Yang Y. and Hu Z. (2016)
Calibration and correction of LA-ICP-MS and LA-MC-ICP-MS analyses for element contents and isotopic ratios. **Solid Earth Sciences**, **1**, 5–27.

McLennan S.M. (2001)
Relationships between the trace element composition of sedimentary rocks and upper continental crust. **Geochemistry Geophysics Geosystems**, **2**, 2000GB0001009.

Mercadier J., Cuney M., Lach P., Boiron M.C., Bonhoure J., Richard A., Leisen M. and Kister P. (2011)
Origin of uranium deposits revealed by their rare earth element signature. **Terra Nova**, **23**, 264–269.

Miller L.J. (1955)
Uranium ore controls of the Happy Jack deposit, White Canyon, San Juan County Utah. **Economic Geology**, **50**, 156–169.

Pagel M., Pinte G. and Rotach-Toulhoat N. (1987)
The rare earth elements in natural uranium oxides. **Monograph Series Mineral Deposits**, **27**, 81–85

Paton C., Hellstrom J., Paul B., Woodhead J. and Hergt J. (2011)
Iolite: Freeware for the visualisation and processing of mass spectrometric data. **Journal of Analytical Atomic Spectrometry**, **26**, 2508–2518.

Pearce N.J.G., Perkins W.T., Westgate J.A., Gorton M.P., Jackson S.E., Neal C.R. and Cheney S.P. (1997)
A compilation of new and published major and trace element data for NIST SRM 610 and NIST SRM 612 glass reference materials. **Geostandards Newsletter: The Journal of Geostandards and Geoanalysis**, **21**, 115–144.

Peńkin M.V., Boulyga S.F. and Fischer D.M. (2016)
Application of uranium impurity data for material characterization in nuclear safeguards. **Journal of Radioanalytical and Nuclear Chemistry**, **307**, 1995–1999.

Petrus J.A., Chew D.M., Leybourne M.I. and Kamber B.S. (2017)
A new approach to laser-ablation-inductively coupled plasma-mass spectrometry (LA-ICP-MS) using the flexible map interrogation tool 'Monocle'. **Chemical Geology**, **463**, 76–93.

Riegler T. and McClenaghan S.H. (2017)
Authigenic potassic silicates in the Rathdowney Trend, southwest Ireland: New perspectives for ore genesis from petrography of gangue phases in Irish-type carbonate-hosted Zn-Pb deposits. **Ore Geology Reviews**, **88**, 140–155.

Sindern S. (2017)
Analysis of rare earth elements in rock and mineral samples by ICP-MS and LA-ICP-MS. **Physical Sciences Reviews**, **2**.

Spano T.L., Simonetti A., Balboni E., Dorais C. and Burns P.C. (2017)
Trace element and U isotope analysis of uraninite and ore concentrate: Applications for nuclear forensic investigations. **Applied Geochemistry**, **84**, 277–285.

Sylvester P. (editor) (2008a)
Laser ablation ICP-MS in the Earth sciences: Current practices and outstanding issues. **Short Course Series**, **40**, **Mineralogical Association of Canada (Vancouver)**, 348pp.

Sylvester P. (2008b)
Matrix effects in laser ablation-ICP-MS. **In: Sylvester P.J. (ed.), Laser ablation ICP-MS in the Earth sciences: Current practices and outstanding issues. Mineralogical Association of Canada**, **40**, 67–78.

Trites A.F. and Chew R.T. (1955)
Geology of the Happy Jack Mine, White Canyon Area, San Juan County, Utah. **US Government Printing Office**.

Walton A.W., Galloway W.E. and Henry C.D. (1981)
Release of uranium from volcanic glass in sedimentary sequences: An analysis of two systems. **Economic Geology**, **76**, 69–88.

Waters O.A. and Granger C.H. (1963)
Volcanic debris in uraniferous sandstones and its possible bearing on the origin and precipitation of uranium. **Geological Survey Circular**, **224 (Report)**, 3pp.

Zhou L., McKenna C.A., Long D.G. and Kamber B.S. (2017)
LA-ICP-MS elemental mapping of pyrite: An application to the Palaeoproterozoic atmosphere. **Precambrian Research**, **297**, 33–55.

Zhou L., Zeng Q., Liu J., Duan X., Sun G., Wang Y. and Chen P. (2020)
Tracing mineralization history from the compositional textures of sulfide association: A case study of the Zhenzigou stratiform Zn-Pb deposit, NE China. **Ore Geology Reviews**, 103792.

Supporting information

The following supporting information may be found in the online version of this article:

Appendix S1. Full measurement results for the Happy Jack and Rum Jungle uraninites as well as NIST SRM 610.

This material is available from: http://onlinelibrary.wiley.com/doi/10.1111/ggr.12457/abstract (This link will take you to the article abstract).